Theses and Dissertations

12-2018

Utilizing the HVSR Second Peak for Surface Wave Inversions in the Mississippi Embayment

Ashraf Kamal Himel

University of Arkansas, Fayetteville

Recommended Citation

Utilizing the HVSR Second Peak for Surface Wave Inversions in the Mississippi Embayment

A thesis submitted in partial fulfillment
of the requirements for the degree of
Master of Science in Civil Engineering

by

Ashraf Kamal Himel
Bangladesh University of Engineering and Technology
Bachelor of Science in Civil Engineering, 2014

December 2018
University of Arkansas

This thesis is approved for recommendation to the Graduate Council.

_____
Clinton Wood, Ph.D.
Thesis Director

_____
Michelle Lee Barry, Ph.D.
Committee Member

_____
Sarah Vavrik Hernandez, Ph.D.
Committee Member

Abstract

Ambient noise data from 24 sites within the Mississippi Embayment were analyzed to estimate the fundamental frequency using the horizontal to vertical spectral ratio (HVSR) method. The fundamental frequency ranged from 0.17 to 3.43 Hz for the tested sites. At seventeen of the sites, a second higher frequency HVSR peak, which ranged from 0.617 Hz to 2.154 Hz, was observed in addition to the fundamental HVSR peak. The second peak frequency in the HVSR curve has been attributed by previous researchers as either an odd harmonic of the fundamental peak or a shallow impedance contrast from the Memphis sand layer in the Mississippi embayment. Shear wave transfer functions are compared for select sites with the HVSR curves and geologic boring logs are analyzed to determine which cause is most likely. Finally, a full scale inversion of active and passive surface wave data is carried out at one site using the HVSR fundamental frequency to constrain the bedrock depth and the second peak frequency to constrain the shallow impedance contrast depth to demonstrate the usefulness of the HVSR second peak.

Acknowledgement

I would like to sincerely thank my supervisor Dr. Clinton Wood. He has been very supportive during this whole journey. I have learned a lot of things in the field of earthquake engineering from him. Finishing up the thesis would not have been possible without his guidance. I am thankful to get the opportunity to work with him.

I would like to thank Dr. Sarah Vavrik Hernandez and Dr. Michelle L. Barry for serving as my thesis committee members. Their teaching has always helped me during my research. I would also thank my teammates in Geotechnical Earthquake Engineering Lab of University of Arkansas.

Dedication

This thesis is dedicated to my family. My father, Abser Kamal has been a great mentor for me throughout my life. My mother, Hasina Jahan has always been beside me. My fiancé, Disha has been patient and supportive the whole time. I would also like to thank my sisters for their continuous support.

Table of Contents

List of Tables

List of Figures

Figure 8: Rayleigh (a) and Love (b) dispersion curves, respectively. Green, red, and blue are for 83 m model, 131 m model, and 171 m model, respectively. Solid line, dotted line and dashed line are for fundamental mode, first higher mode and second higher mode of theoretical

1.0 Introduction:

The horizontal to vertical spectral ratio (HVSR) method, also known as the Nakamura's method (Nakamura 1989) is widely accepted as a tool to evaluate site effects (Guéguen *et al*. 2000). The HVSR peak frequency emulates the resonance frequency or fundamental frequency (f_0) of sediments above a strong impedance contrast and is equated to the shear wave fundamental frequency (Field and Jacob 1993). The peak frequency is related to the sediment thickness, while the amplitude is related to the shear wave velocity contrast between the top sediments and stiff base material (Guéguen *et al*. 1998). While at many sites one primary peak is often observed in the HVSR curve from only one major impedance contrast (Bonnefoy-Claudet et al., 2008), the presence of two interfaces with significant impedance contrasts may generate two peaks in the HVSR curve (Guéguen *et al*., 2000).

Two peaks in the HVSR curve have been observed in a number of locations around the world. Zaslavsky *et al.*, (2007) correlated the HVSR first peak frequency with the limestone bedrock and the second peak frequency with the shallow softer alluvial sediments in Zevulun plain, Israel. They showed that the HVSR second peak varied from 17 Hz down to 4 Hz, matching the increase of alluvial layer thickness from 2 m to 15 m. Macau *et al*. (2015) conducted a study on the effect of Quaternary deposits on HVSR at Llobregat river delta, located to the south of Barcelona. In this study, they detected two impedance contrasts along with two peaks in the HVSR curves. The first peak was correlated with the deeper impedance contrast between soft sediment and bedrock, while the second peak was correlated with the shallow impedance contrast between soft clay and gravel, concluding that the structure of shallow quaternary layer can change the shape of H/V ratio by producing two clear peaks. Wotherspoon et al. (2018) showed that the first HVSR peak in the Canterbury Plains, New Zealand was the

1

result of basement rock, while the second HVSR peak was correlated with a soft sand layer over a stiff gravel layer located 10-40 m below the surface.

The existence of a second HVSR peak can also have a significant influence on the seismic site effects for a particular location. For Pujili (Ecuador), the damage distribution due to the Mw 5.7 earthquake in 1996 showed most of the damaged buildings had similar natural frequency as the HVSR second peak frequency. The second peak frequency in Pujili was found to be the resonant frequency of a superficial thin layer (Field and Jacob 1993). The damage due to the earthquake on May 21, 2003 hitting the eastern coast of Algiers also demonstrated a similar condition. The first peak, around 1 Hz in the HVSR curve, could not explain the building collapses, which had natural frequencies in the range of $3 - 4$ Hz. A second HVSR peak around 3 Hz was observed in this case, which was correlated with the shallow impedance contrast between quaternary and Mio-Pliocene layer (Dunand *et al*., 2004, Guillier *et al.*, 2005).

The Mississippi embayment, situated in the Central United States, is a deep sedimentary basin in which two HVSR peaks are often observed (Rosenblad and Goetz 2010 Bodin *et al.*, 2001, Wood *et al.*, 2018, Guo and Aydin 2016, Guo *et al.*, 2014, Carpenter *et al.*, 2018). Bodin et al. 2001 hypothesized that the second peak frequency (f_1), is a harmonic of the fundamental peak as the ratio f_1/f_0 was found to be near 3 and they could not identify an impedance contrast strong enough to cause the second peak. Moreover, Goetz (2009) generated shear wave transfer functions using Vs profiles from Rosenblad *et al.*, 2010 to show that the shear wave transfer function second peak is in good agreement (<10%) with the measured HVSR second peak. They suggested that this could be a reason to consider the second peak frequency as a higher mode of shear wave resonance. However, they also used the shear wave transfer function down to the Memphis sand layer to show a relationship of decreasing resonance frequency with increasing

depth to the top of Memphis sand, indicating that the velocity contrast also could be the cause of second peak frequency observed in the HVSR across the embayment similar to that observed in many other basins around the globe. There is still uncertainty regarding the cause of the second higher frequency HVSR peak observed throughout the embayment primarily due to the fact that the higher frequency HVSR peak is often about three times the fundamental HVSR peak associated with the bedrock formation, but also that the depth to the Memphis sand layer (the presumed shallow impedance contrast) often decreases at a similar rate to the bedrock depth across the embayment. This make is difficult to isolate the true cause of the second HVSR peak across the region. Regardless of the cause of the second HVSR peak, the site effects which result as a function of the amplification at the HVSR second peak frequency play a key role in the seismic hazard of the region. However, if the second peak is a result of an impedance contrast at the top of the Memphis Sand, this HVSR peak can be used in the solution of the inverse problem in surface wave methods through a joint inversion to constrain the V_S of the sediments, resulting in a more accurate Vs profile (Scherbaum *et al*. 2003). Therefore, aiding in the assessment of seismic hazard in the region.

In this paper, the HVSR second peak frequency observed in the Mississippi embayment is associated with the shallow impedance contrast from the Memphis sand and the ability to use this second HVSR peak frequency along with dispersion data from surface wave methods to resolve the depth to the Memphis sand is demonstrated. Direct ambient noise measurements are used to compute HVSRs at 15 sites across North East Arkansas and then compared to shear wave transfer functions computed using V_S profiles from Wood et al. (2018). Next HVSRs are computed at nine sites at the western and northern edges of the embayment and compared to boring logs and geologic cross sections which indicate the Memphis sand layer no longer exist

along the basin edges. Finally, the use of the HVSR second peak to constrain the inversion of active and passive surface wave dispersion data is demonstrated for a site within the embayment.

 ## 2.0 Mississippi Embayment Geology

The Mississippi embayment is a southward plunging syncline, with its axis closely tracing the course of the Mississippi river (Mento *et al*. 1986). The embayment has a rift type crustal structure (Ginzburg *et al*. 1983) and the subsidence of the rift formed the Reelfoot Basin in early Paleozoic (Schwalb 1971). One of the geologic characteristics of Mississippi embayment is its deep, unconsolidated sedimentary deposits. The sedimentary deposit depth can extend from approximately 150 m in Jackson County, MO to 1100 m in Lee county, AR (Dart 1995). The surface deposits within the basin are mainly classified as Holocene or Pleistocene (Romero *et al*. 2005), while the bedrock is Knox Dolomite from the Paleozoic era (Cushing *et al*. 1964). The Memphis sand and the Paleozoic bedrock are the two main impedance contrasts in the Mississippi Embayment (Rosenblad et al. 2010). The alluvial surface deposits have a low shear wave velocity (V_S) of 193 ± 14 m/sec compared with the shear wave velocities of the Memphis sand and Paleozoic bedrock units, which are 685 ± 83 m/sec (Rosenblad *et al*. 2010) and 2000 - 3400 m/sec (Cramer 2006), respectively. Clay, silt, sand, gravel, chalk, and lignite fill up the embayment, with ages ranging from Cretaceous to recent Holocene (Hashash *et al*. 2010).

Quaternary, Tertiary, Upper Cretaceous, and Paleozoic era geologic strata are main constituents of the Mississippi Embayment's geology (Van Arsdale *et al*. 2000).   In the uppermost Quaternary layer, the surface deposits are mainly classified as Holocene or Pleistocene (Romero *et al*. 2005). Holocene deposits are mainly found in the alluvial plains of the Mississippi River floodplain, also known as the lowlands and Pleistocene deposits are found further inland on the highlands (Romero *et al*. 2005). As shown in Figure 1, the Lowlands are

situated to the west of the Mississippi River and the highlands are situated to the east. Crowley's Ridge, which is located in the lowlands, is a Pleistocene-age deposit, which rises 60 meters above the alluvial plane (shown in Figure 1, Van Arsdale *et al*. 2000). The Upper Tertiary layer is situated below the Quaternary layer, consisting of the Jackson formation and the upper Claiborne group. The Jackson formation consists of clay, silt, sand and lignite (Brahana *et al*. 1987), whereas the upper Claiborne includes Cockfield and Cook Mountain formation, characterized by silts and clay (Van Arsdale *et al*. 2000). Lower to Middle Claiborne group (LMC) is found below the Upper Tertiary layer. The Memphis sand unit is a part of the LMC, which is a very fine to coarse grained and light gray-white sand (Van Arsdale *et al*. 2000). Memphis sand, also known as the "500 feet sand" (Romero *et al*. 2005), is the principle aquifer for the Memphis area. This unit can be 164-292 m thick and is approximately 300 m deep in the Memphis area (Brahana *et al*. 1987). The Tertiary is subdivided into two units because of the shear wave velocity contrast between the Memphis sand in LMC and Jackson, Cockfield, and Cook Mountain in Upper tertiary. The Paleocene layer is situated below LMC and contains the Wilcox and Midway groups. Above the bedrock is the Cretaceous layer. This layer consists of McNairy sand layer, the Demopolis Formation, and the Coffee Formation (Van Arsdale *et al*. 2000). The bedrock in Mississippi Embayment is Knox Dolomite from Paleozoic era (Cushing *et al*. 1964).
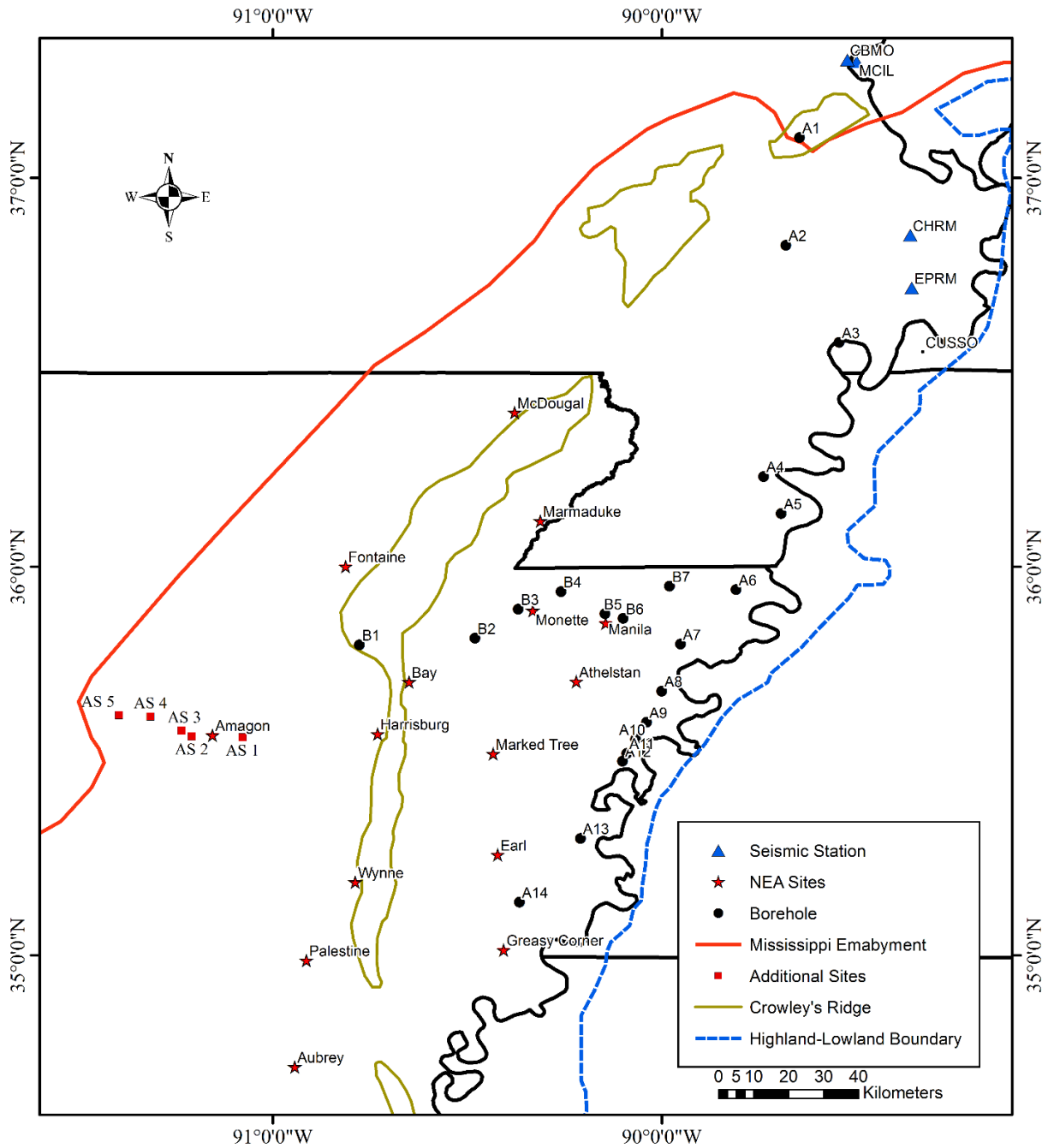
Figure 1. Location of HVSR measurement sites in the Mississippi Embayment along with the seismic stations and boreholes from Ryling (1960) used in this study.

3.0 Testing Methodology and Data Processing

For this study, HVSR measurements were made at 20 sites throughout the Arkansas portion of the Mississippi Embayment. Measurements at 15 of these sites were completed as part of a larger project to characterize the Vs structure of the Arkansas portion of the Mississippi

6

Embayment using active and passive surface wave methods (Wood *et al*., 2018). These 15 sites

are shown as NEA sites in Figure 1. HVSR measurements were made at six additional sites in

the Lowlands as shown in Figure 1. These additional sites were collected to fill in data gaps in

the western portion of the embayment. In addition, HVSR analysis were made using seismic

station data (Incorporated Research Institutions for Seismology). Data from the EPRM, CHRM,

MCIL, and CBMO seismic stations were selected for this study. In Table 1, the location and

bedrock depth, determined from the Central US Velocity Model (CUSVM) developed by

Ramirez *et al* (Ramírez-Guzmán *et al*., 2012), are listed for each site.

Table 1 Site locations and Bedrock depth (Ramirez *et al.*, 2012).

Site Type	Name	Latitude	Longitude	Bedrock Depth(m)
NEA Site	McDougal	36.398583	-90.388175	252
	Fontaine	36.017175	-90.799475	291
	Amagon	35.567572	-91.155928	326
	Marmaduke	36.118611	-90.313083	492
	Bay	35.761622	-90.594256	587
	Monette	35.885581	-90.335186	677
	Harrisburg	35.565781	-90.730197	701
	Manila	35.852500	-90.147089	813
	Marked Tree	35.520050	-90.435811	853
	Wynne	35.188317	-90.789519	853
	Athelstan	35.704214	-90.217497	858
	Palestine	34.986725	-90.911181	958
	Earle	35.258642	-90.422603	1018
	Greasy Corner	35.015908	-90.403436	1069
	Aubrey	34.711003	-90.943864	1114

Table 1 (Cont.)

Site Type	Name	Latitude	Longitude	Bedrock Depth(m)
AS	AS 1	35.561	-91.07799	392
	AS 2	35.56388	-91.20834	392
	AS 3	35.57840000	-91.234630	253
	AS 4	35.61482	-91.31445	171
	AS 5	35.61861	-91.39546000	112
	AS 6	35.725917	-91.627005	40
Seismic Station	EPRM	36.717	-89.358	454
	CHRM	36.852567	-89.362014	304
	MCIL	37.298775	-89.499895	20
	CBMO	37.30363	-89.52365	20

3.1 Testing Methodology:

Ambient vibrations were recorded at each measurement site using three component Nanometrics Trillium Compact Broadband Seismometers. These seismometers have a flat frequency response from 0.05 Hz to 100 Hz and a tilt tolerance of 10 degrees. HVSR data at the NEA sites were collected as part of microtremor array measurements made at site where 10 seismometers were used to form circular arrays with diameters between 50-1000 m in diameter. HVSR data was collected for approximately five hours at each site between the different array setups. The seismometers were installed in 15 centimeter diameter and $15 - 30$ centimeter deep holes to reduce uncorrelated noise. Each seismometer was recorded using a Centaur Digitizer with a sampling rate of 100 Hz. For the additional sites in this study, two seismometers were used ambient vibrations for approximately 30 mins at each location.

In addition to the HVSR measurements, active source Multi-Channel Analysis of Surface Wave (MASW), circular and L-array Microtremor Array Measurement (MAM) were also carried

out to generate Vs profiles at the site. Details regarding these measurements and further details regarding the HVSR measurements can be found in Wood *et al*., (2018) and Deschenes *et al*., (2019).

3.2 HVSR Processing:

The time domain data of each component and sensor were divided into 180 second windows. Depending on the recording length, $10 - 100$ windows were selected to transform the time domain data to the frequency domain using the Fourier transformation. Fourier spectra were smoothed using Konno & Ohmachi (1998) smoothing filter, with the parameter b set equal to 40. The geometric mean of the horizontal amplitude spectra were used. HVSR curve for each window was produced from the ratio of the final horizontal spectrum to vertical spectrum. The results from all windows were used to produce an average peak. If the HVSR peaks were consistent between all sensors, the peaks were combined to provide a single HVSR peak with associated standard deviation for each site. Geopsy software package was used for the HVSR calculations. SESAME guidelines were followed for selecting the peaks and overall HVSR processing. Details of the HVSR peak selection and processing guidelines could be found in SESAME 2004.

4.0 HVSR Results

HVSR results from 15 NEA sites are shown in Figure 2. The sites in this figure are sequentially organized from (a) through (o) with increasing bedrock depth. The shallowest bedrock depth is 252 m for McDougal site and the deepest bedrock depth is 1114 m for Aubrey site (Ramírez-Guzmán *et al*. 2012). The HVSR results show that the fundamental frequency (f_0) decreases with increase of bedrock depth (Scherbaum *et al*., 2003, Arai and Tokimatsu 2005). Maximum f_0 is 0.616 Hz for the shallowest site McDougal and the minimum f_0 is 0.186 Hz for

9

the deepest site Aubrey. Theoretical transfer function for vertically propagating, horizontally polarized shear waves (TF) are calculated for each site using the shear wave profile from Wood *et al*., 2018. The TFs are calculated using MATLAB codes (Teague *et al*., 2018). These TFs are shown together with the HVSR curves for each site in Figure 2. For all 15 sites, the fundamental frequency peak of the HVSR matches well (between 1-14% differences) with the TF first peak (Wood *et al.*, 2018).

For 13 of the NEA sites, a second peak can be observed in the HVSR curve. However, the TF second peak only corresponds well with the HVSR second peak at three sites (Marmaduke, Earle and Greasy Corner). The fundamental and second HVSR peak frequencies for the 15 sites are shown in Figure 3 as a function of sediment thickness. In addition, the ratio of the second peak frequency to the fundamental peak frequency, f_1/f_0 are plotted with their corresponding sediment thicknesses in Figure 3. For the 13 sites with HVSR second peaks, the ratio of f_1/f_0 is approximately 3 (the odd harmonic of the first mode of vibration) for only three of the sites. The majority of the sites have ratios greater than 3.5-4.0 with a minimum value of 2.7 and maximum value of 5.21 for Aubrey and Amagon, respectively. This suggests that the HVSR second peak is not an odd harmonic of the fundamental peak, but a function of a shallower impedance contrast as is true at many other basins.
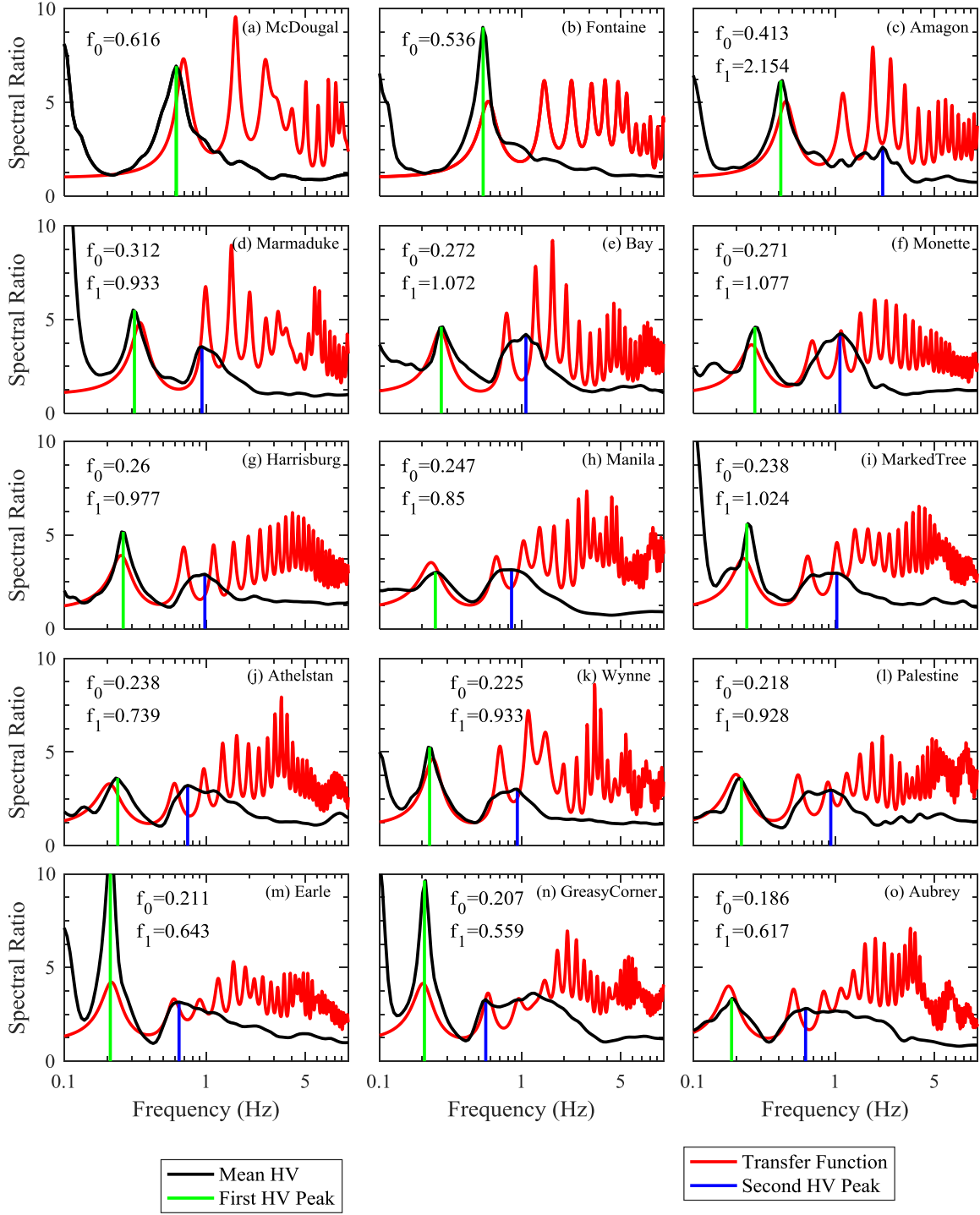
Figure 2: HVSR curve for the 15 NEA sites in the study compared with the theoretical shear wave transfer function. The associated peaks are highlighted.
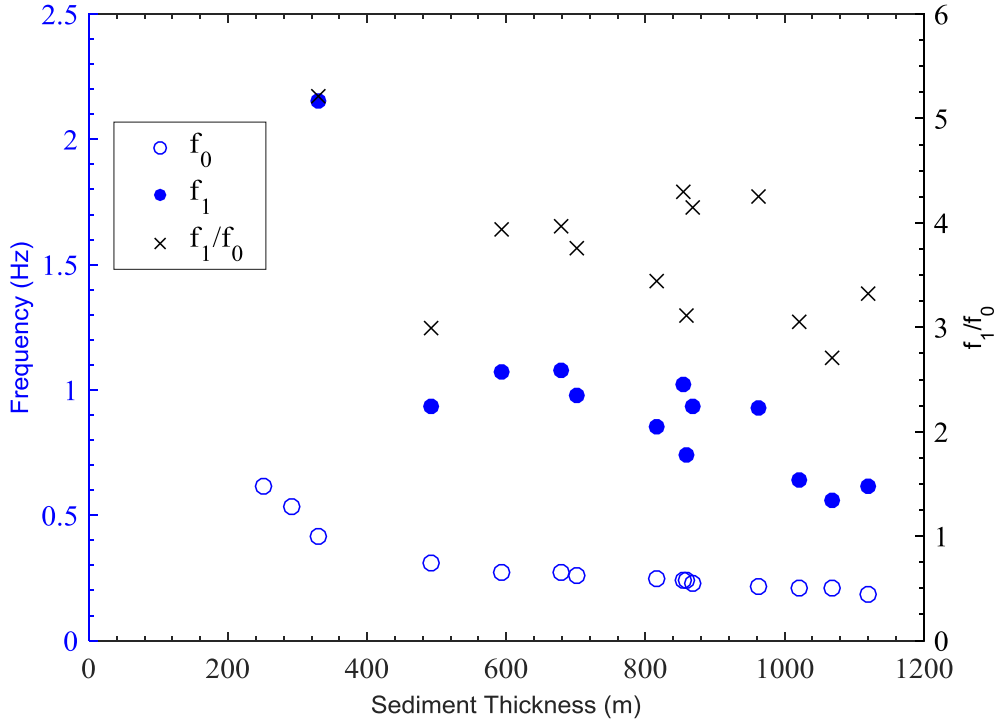
Figure 3: HVSR fundamental and second peak frequencies for the 13 NEA sites with second peaks (Blue hollow are fundamental peak and blue filled points are second peak frequencies). The ratio of the second peak frequency to the first peak frequency is also shown on the right axis.

To understand the prevalence of the second HVSR peak spatially across the Mississippi Embayment, borehole logs and cross sections are presented from Ryling 1960 in Figure 4. A total of 21 boreholes from Oran, Missouri to Jennette, Arkansas in north-south direction (Figure 4a) and Gosnell, Arkansas to Jonesboro, Arkansas in east-west direction (Figure 4b) are shown. Locations of the boreholes are shown in Figure 1. The LMC (Memphis sand) depth from the CUSVM are also added to the cross sections (shown as CUSVM LMC) in Figure 4. The northern most borehole A1 in Figure 4 (a) indicates no Claiborne group exist this far north, whereas A2 through A14 show the existence of the Claiborne group. The Claiborne group is shown to exist in boreholes B1 through B7 and ends somewhere west of B1. In conglomeration, Figure 4 shows that the Claiborne group along with the Memphis sand becomes shallower moving northwards and westwards to the embayment boundary and diminishes gradually.

The Memphis sand layer (part of the Claiborne Group) has been established as strong impedance contrast at shallow depth within the Mississippi Embayment (Rosenblad *et al.*, 2010, Gomberg *et al.*, 2003, Williams *et al.*, 2003). From Ryling 1960 (Figure 4), the approximate locations where the Claiborne group exists within the Embayment have been identified. The general trend of Claiborne group is that, it gradually becomes shallower moving towards the north and the west boundary of the Mississippi embayment and expires at some point. To observe the change of HVSR peaks moving northwards, HVSR analysis was carried out on data from four seismic stations (EPRM, CHRM, CBMO, and MCIL). The location of these stations are shown in Figure 1. Figure 5 (a) through 5 (d) shows the HVSR results of EPRM, CHRM, CBMO, and MCIL, respectively. Seismic stations within the embayment, EPRM and CHRM have multiple HVSR peaks and the first peaks are around 0.38 Hz and 0.51 Hz, respectively with the second peaks at 0.89 Hz and 1.48 Hz, respectively. This results in a ratio of 2.34 and 2.9 (both <3) between f_1/f_0 respectively for EPRM and CHRM. EPRM and CHRM are to the east of borehole A2, which contains Claiborne group. Stations outside of the embayment are CBMO and MCIL, where CBMO shows a small second peak and MCIL has only the fundamental peak. Both CBMO and MCIL are to the north of A1, which doesn't contain any Claiborne group as the Claiborne group disappears somewhere between A2 and A1. Fundamental peaks for CBMO and MCIL are around 3.43 Hz and 2.3 Hz, respectively. The HVSR results from four seismic stations near the northern boundary of the embayment show that the HVSR second peak diminished gradually moving northward. Sites AS1 through AS5 are near the western boundary of the Mississippi embayment (Figure 1). HVSR results from these sites show the gradual change of the peaks in the HVSR when moving westward (in Figure 6). AS1 and AS2 show two peaks, where the second peak of AS1 is not very prominent.
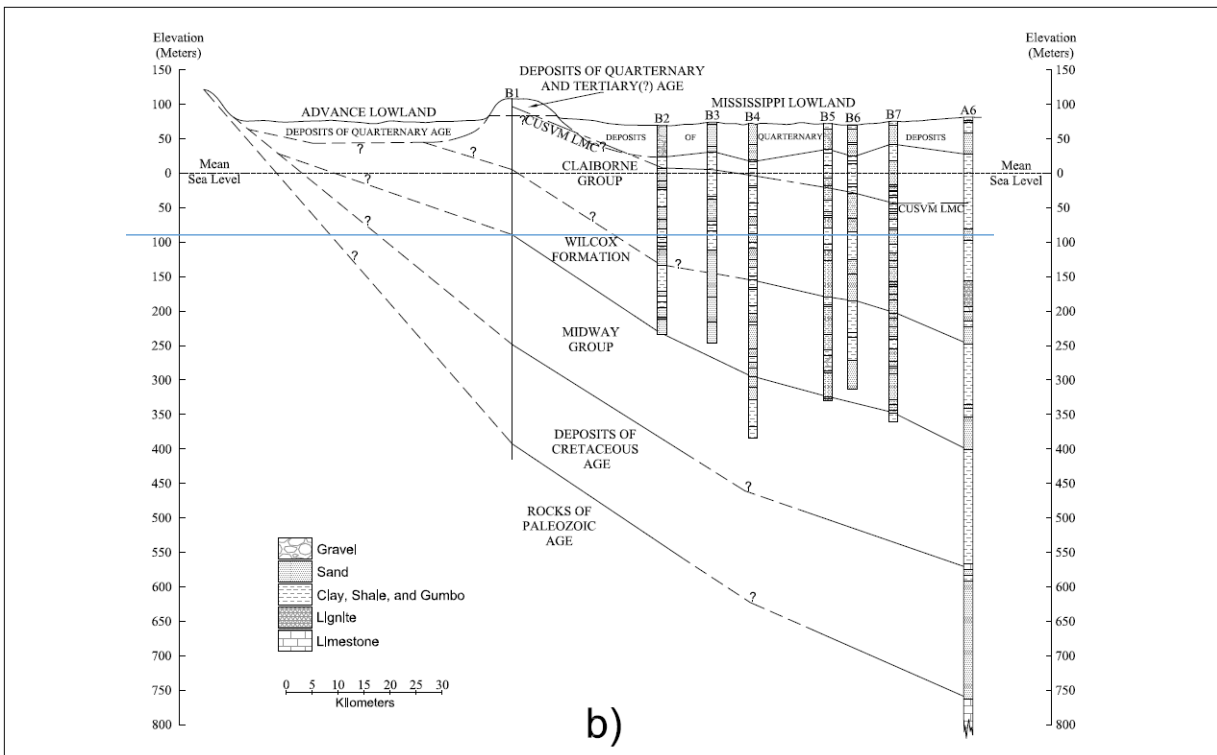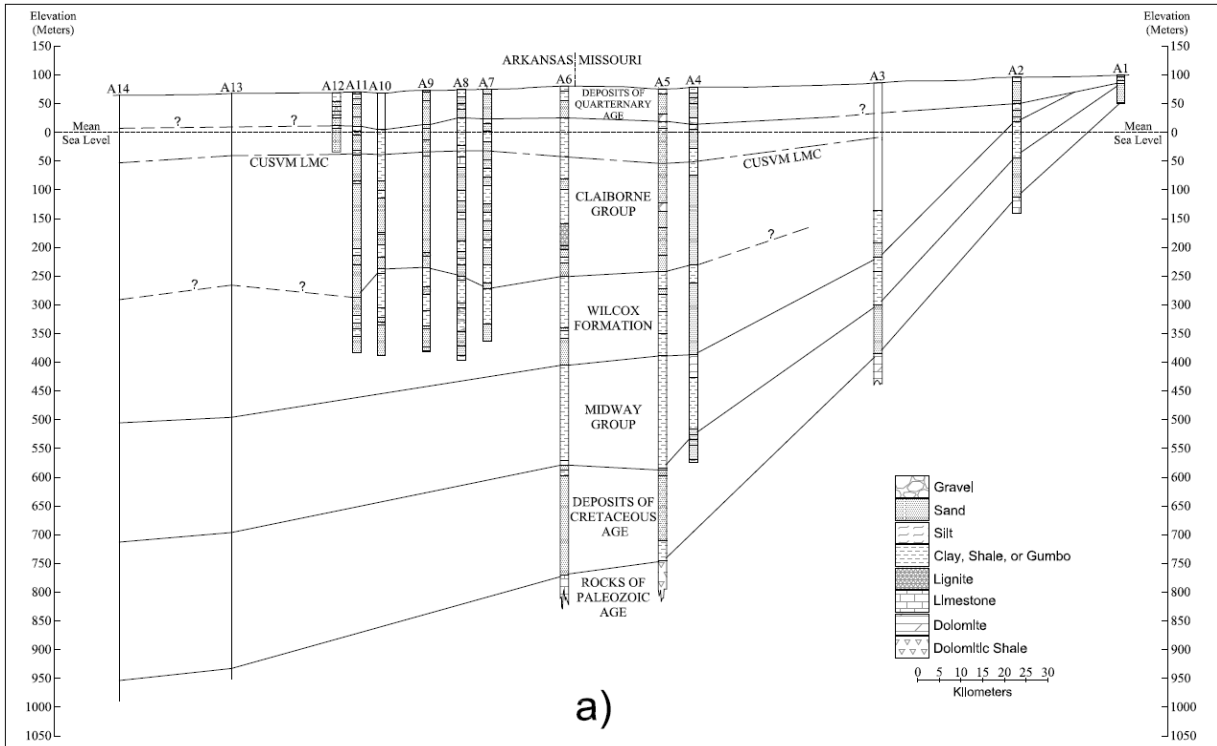
Figure 4: Generalized geologic cross section of the Mississippi embayment from boreholes originally presented in Ryling (1960): (a) North-South cross section for boreholes A1 – A14 and (b) East-West cross section for boreholes B1 – B7.

14

Fundamental peak of AS1 and AS2 are 0.36 Hz and 0.53 Hz, respectively. The f_1/f_0 ratio for

AS1 and AS2 are respectively 2.78 and 3.36. AS3, AS4, and AS5 sites have only fundamental

peaks at 0.39 Hz, 1.12 Hz, and 2.24 Hz, respectively. Thus, it could be inferred that the HVSR

second peak in the Mississippi embayment exists where shallow impedance contrast from

Memphis sand layer is present and disappears with the disappearance of the Memphis sand layer.
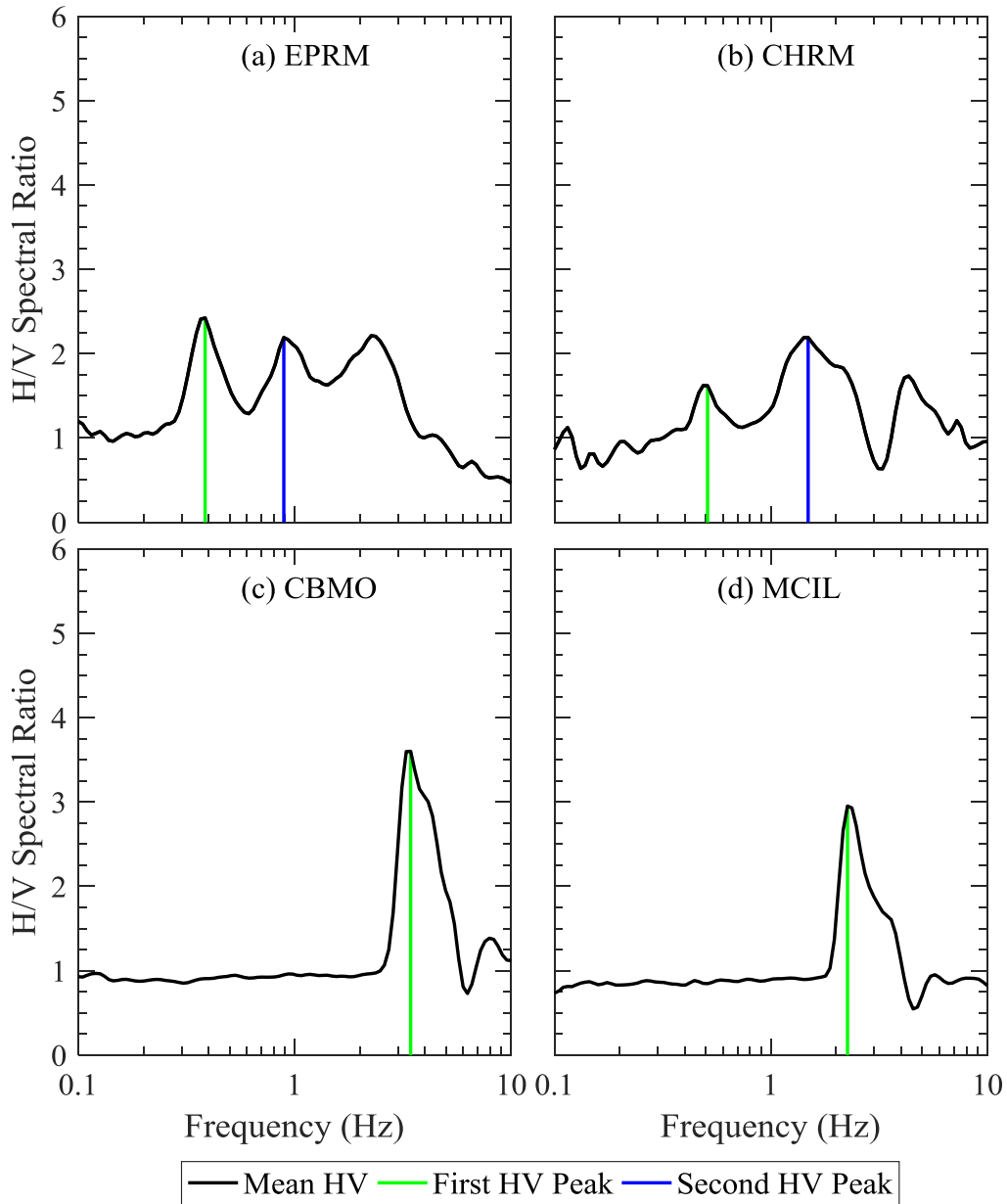
Figure 5: HVSR result of seismic stations EPRM, CHRM, CBMO, and MCIL.
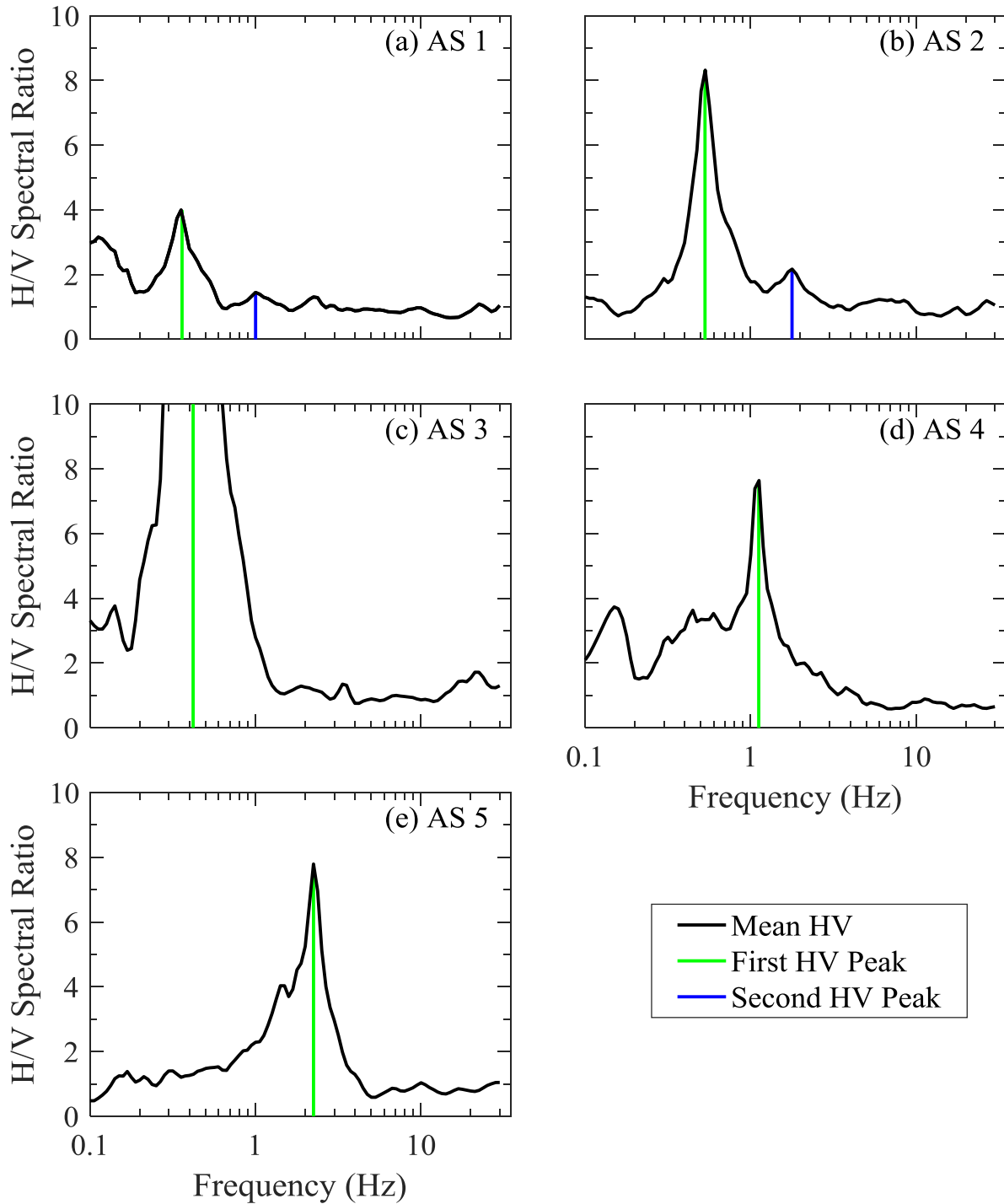
Figure 6: HVSR results of the Additional Sites along the western edge of the Mississippi Embayment.

Table 2 shows the second peak frequency and fundamental frequency along with the f_1/f_0 ratio for the 17 sites with HVSR second peak. The average of f_1/f_0 ratio of the 17 sites is found to

be 3.5 Hz with a sample standard deviation of 0.733 Hz. A hypothesis test on the population

mean of f_1/f_0 was carried out, where

Null hypothesis, H_0: Population mean of f_1/f_0, $\boldsymbol{\mu} = 3.0$

Alternative hypothesis, H_1: Population mean of f_1/f_0, $\mu \neq 3.0$

Now using the equation, $t = \dfrac{\bar{x} - \mu}{s/\sqrt{n}}$

Where, t=test statistics, $\bar{x}$ =sample mean, μ =population mean, s =sample standard

deviation, n =number of samples. The test statistics, t was found to be 2.81, which is greater

than the critical value of a two tailed t distribution at 5% level of significance, t_c=2.120. Thus,

the null hypothesis is rejected that the population mean is equal to 3.

Applying Students t test on the f_1/f_0 ratio, the lower and upper bound for population mean of

f_1/f_0 are found to be 3.124 Hz and 3.876 Hz, respectively at 95% confidence interval. This

indicates that there is 95% certainty that the population mean of f_1/f_0 will be between 3.124 Hz

and 3.876 Hz, indicating the ratios of the peaks is not three and likely not the result of odd

harmonics.

Table 2 Second peak frequency and fundamental frequency along with their ratio, for the sites
with HVSR second peak.

Site Type	Name	f_0 (Hz)	f_1 (Hz)	f_1/f_0
	Amagon	0.413	2.154	5.22
	Marmaduke	0.312	0.933	2.99
	Bay	0.272	1.072	3.94
NEA Sites	Monette	0.271	1.077	3.97
	Harrisburg	0.26	0.977	3.76
	Manila	0.247	0.85	3.44
	Marked Tree	0.238	1.024	4.30

Table 2 (Cont.)

Site Type	Name	f_0 (Hz)	f_1 (Hz)	f_1/f_0
	Athelstan	0.238	0.739	3.11
	Wynne	0.225	0.933	4.15
	Palestine	0.218	0.928	4.26
	Earle	0.211	0.643	3.05
	Greasy Corner	0.207	0.559	2.70
	Aubrey	0.186	0.617	3.32
AS	AS1	0.36	1.001	2.78
	AS2	0.53	1.78	3.36
Seismic Station	EPRM	0.38	0.89	2.34
	CHRM	0.51	1.48	2.90

5.0 Inversion Results at Manila, AR

The Manila site is located in the Mississippi County, Arkansas, which is geologically situated in the lowlands. As per Dart 1995, the depth to bedrock for Manila is around 750 m, whereas the CUSVM indicates a depth of 813 m (Ramírez-Guzmán *et al*., 2012). The Memphis sand depth at this site is at 83 m and around 200 m as per CUSVM and Ryling 1960, respectively. For shear wave velocity profiling at this site, a combination of active source multi-channel analysis of surface wave (MASW), passive source Microtremor array measurements (MAM) and horizontal to vertical spectral ratio (HVSR) measurements were carried out. The active source MASW was carried out using 24, 4.5 Hz geophone with 2 m spacing using both vertical (Rayleigh) and horizontal (Love) geophones. A 4.5 kg hammer was used for the vertical and horizontal impact to generate Rayleigh and Love wave, respectively. For ensuring high quality data and minimizing near field effects, source offset of 5 m, 10 m, 20 m, and 40 m were used from the first geophone of the array. At each source offset location, 10 vertical/horizontal impacts were

stacked to increase the signal to noise ratio. MAM measurements were made using circular

arrays of 50 m, 200 m, and 500 m diameter. Three component Nanometrics Trillium Compact

20 s broadband seismometers were used. In each array, one seismometer was placed at the

center of the array and nine uniformly distributed around the circumference. Ambient noise was

recorded for one hour for the 50 m and 200 m diameter arrays and for two hours for the 500 m

diameter array.

The Rayleigh and Love wave MASW data were processed using the multiple-source offset

technique combined with the Frequency Domain Beamformer (FDBF) method (Zywicki et al.,

1999, Cox et al., 2011). Rayleigh wave dispersion data from vertical component of ambient

noise, recorded from the circular arrays were processed using the High-Resolution Frequency

Wavenumber (HRFK) method (Capon 1969) and the Modified Spatial Auto-Correlation

(MSPAC) method (Bettig et al., 2001). Love wave data from MAM were also processed using

the HRFK processing. The individual curves from each method and arrays (MAM) were first

cleared of outlying points. Then a composite dispersion curve was produced combining the

dispersion curves from each method (Park et al., 1999, Foti et al., 2014). This composite

dispersion curve along with the HVSR peak were used to make a joint inversion in the Geopsy

software package Dinver. Details of the dispersion processing could be found in Wood et al.,

2018.

The f_0 and f_1 HVSR peaks for the Manila site are respectively 0.247 Hz and 0.85 Hz with a

f_1/f_0 ratio of 3.44 (>3.0). From Ryling 1960, two borehole B5 and B6 are located close to the

Manila site, respectively 2.65 km to the east and 4.2 km to the north-east of Manila. From the

borehole logs, it was estimated that B5 and B6 has the Memphis sand layer starting from 200 m

and 220 m, respectively. Utilizing this borehole information and CUSVM, a preliminary idea

about Memphis sand depth at the Manila site was estimated to be around 80-200 m.

Figure 7 (a) through (c) illustrates three separate shear wave velocity models for Manila.

The 83 m model, shown in Figure 7 (a) is generated by Wood *et al*. 2018 by joint inversion of

the dispersion data and HVSR fundamental peak. For this model, layer parameterization was

created using CUSVM (Ramírez-Guzmán *et al*. 2012) geologic unit boundaries and a subset of

layers to allow varying layer thickness. V_s, and V_p ranges for the parameterization for each layer

is based on Lin *et al*., 2014, Romero and Rix 2005, Rosenblad *et al*., 2010, Ramírez-Guzmán *et

al*., 2012, and Woolery *et al*., 2016. The model shown in Figure 7 (a) demonstrates the potential

Memphis sand layer to start from 83 m, which is coherent with the CUSVM Memphis sand

depth at this location.

To resolve the Memphis sand depth more accurately in the V_S profile, two more V_s models

were generated in this paper. For these models, the inversions were carried out in two phases. In

the first phase, instead of the fundamental frequency, the HVSR second peak frequency was used

to constrain the Memphis sand depth. The same parameterization used for the 83 m model was

used down to the predicted Memphis sand depth. Dispersion data along with the HVSR second

peak was inverted. In the second phase, the resulting V_s profile from the first phase was used to

constrain the parameterization down to the Memphis sand depth found in the first phase. The

remainder of the parameters were same as Wood *et al*., 2018. As the second phase is a full scale

inversion down to the bedrock, the fundamental peak was used along with the dispersion data.

For the 131 m model, the first phase inversion was conducted using the 83 m model

parameterization down to 200 m (preliminary estimation of Memphis sand depth) and using the

HVSR second peak at 0.85 Hz. This resulted in demonstrating the Memphis sand depth around

130 m. For the phase two inversion, the first phase inversion result was utilized to constrain the parameterization down to 130 m by narrowing down the shear wave velocity ranges. Rest of the parameterization was the same as the 83 m model. The fundamental HVSR peak of 0.247 Hz was used to constrain the bedrock depth. The phase two inversion resulted in the Memphis sand at 131 m as shown in the Figure 7 (b). A third Vs model was formed following the same procedure. Only this time, in the first phase inversion, the Memphis sand was forced to be between 170 - 200 m depth by constraining the Vs range in this depth range. The final result after the phase two inversion resulted in the Memphis sand layer at a depth of 171 m as shown in Figure 7 (c). All three models were produced using 2 million neighborhood algorithm solutions. The 1000 best misfit solutions from the 2 million were selected and shown for each model. The median V_s profile from the best 1000 misfit profiles were calculated and shown as the thick red line in corresponding models.

The median V_s profile from each model was used to produce the theoretical dispersion curve for each corresponding model as shown in Figure 8. Figure 8 (a) shows the theoretical Rayleigh dispersion curve along with the Rayleigh experimental data. Figure 8 (b) shows the theoretical Love dispersion curve along with the Love experimental data. Figure 8 (a) demonstrates that the 131 m model and 171 m model fundamental mode starts separating from the 83 m model fundamental mode around 1.77 Hz. The phase velocity at 1.77 Hz is around 492 m/sec, which corresponds to a depth of approximately 139 m. The fundamental mode of the 131 m model and 171 m model are almost identical. The minimum misfit for 83 m model, 131 m model, and 171 m model inversion results are respectively 0.79, 0.37, and 0.47. The misfit is a function of the difference between the theoretical and experimental ellipticity peaks and difference between the experimental and theoretical dispersion data at each frequency point (Deschenes *et al.*, 2019).
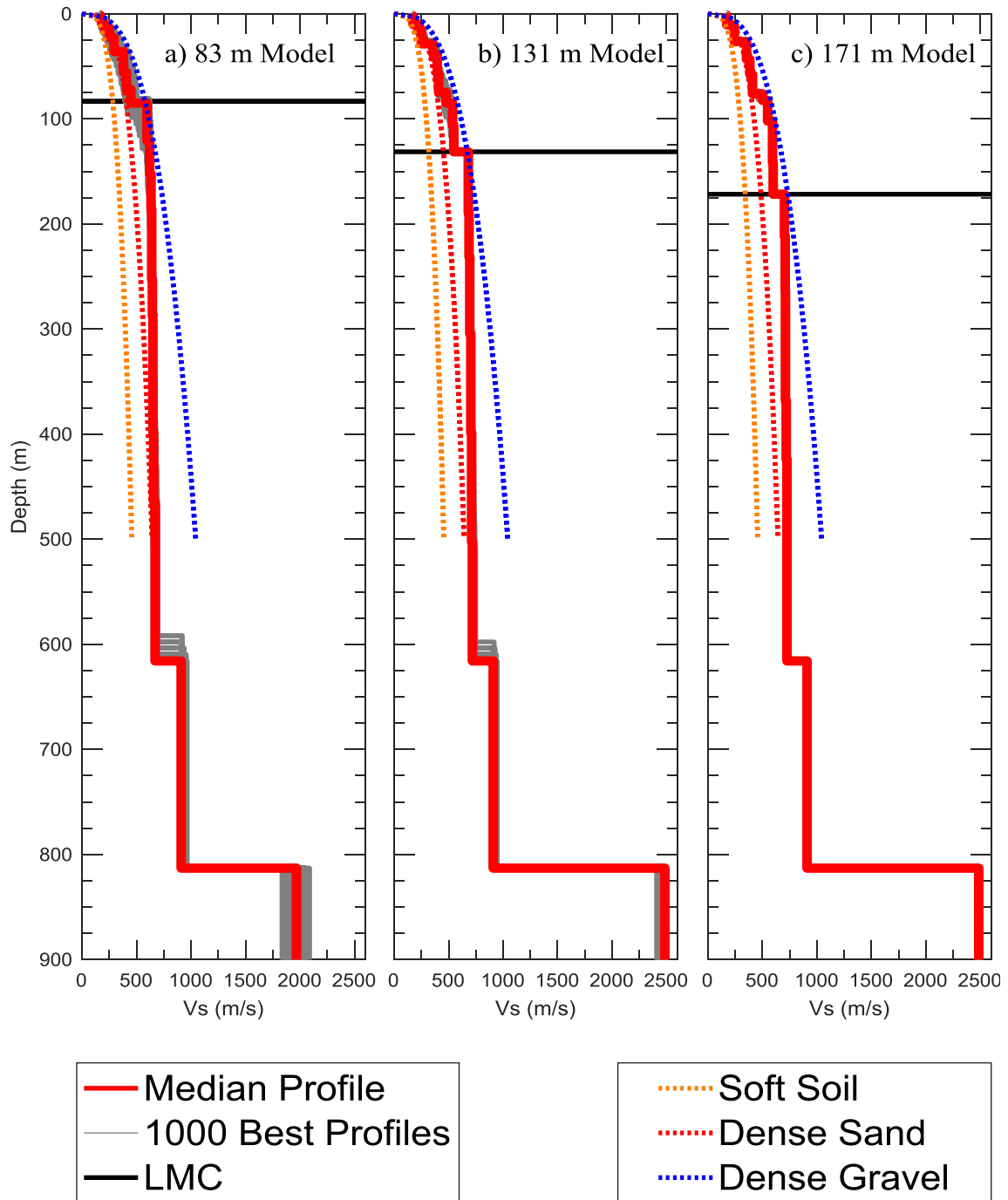
Figure 7: Median Vs profiles of the 83 m model, 131 m model and 171 m model along with the 1000 Vs best profiles are shown. For each model, the estimated Memphis sand depth is shown with the thick black line. Reference Vs profiles of Lin *et al*., 2014 for different soil types are provided for comparison

The misfit values are dependent on the quality and quantity of dispersion data and the

complexity of the geology (Teague et al., 2017). Along with the quantitative misfits, visual fit

quality was also inspected. The minimum misfit of the 83 m model is highest among all three

models. This is because the other two models were able to fit better with the experimental data around 1.77 Hz, which also made these two models stiffer than the 83 m model from around 130 m reflecting the impedance contrast. The inset in Figure 8 (a) shows that the 131 m model and 171 m model are visually fitting better with the experimental data than the 83 m model.
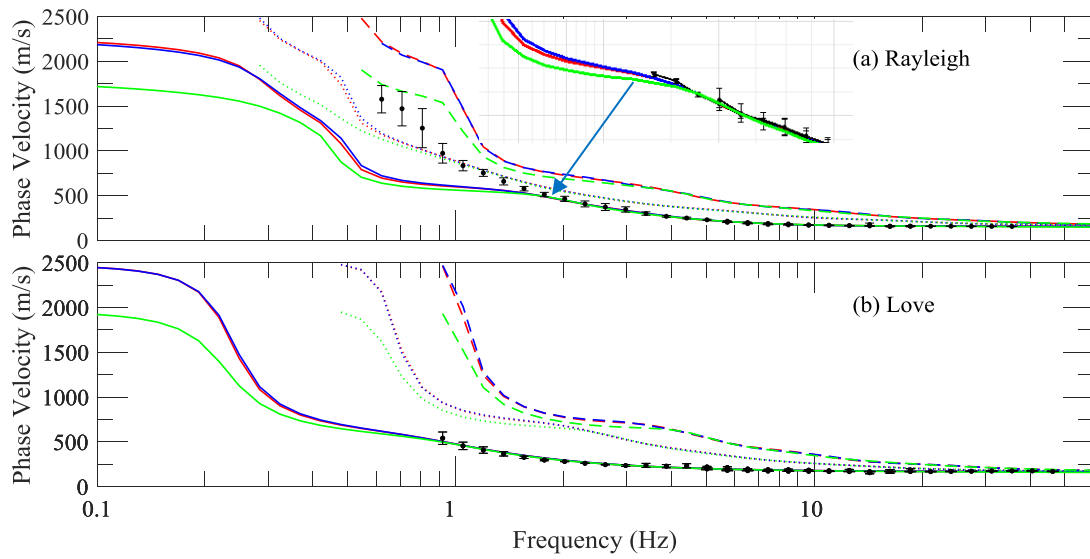

Figure 8: Rayleigh (a) and Love (b) dispersion curves, respectively. Green, red, and blue are for 83 m model, 131 m model, and 171 m model, respectively. Solid line, dotted line and dashed line are for fundamental mode, first higher mode and second higher mode of theoretical dispersion curves, respectively. The black dots are experimental dispersion data. The inset in (a) shows an enhanced image of the fundamental mode dispersion data from 0.5 Hz to 2.5 Hz. The inset shows the separation of 131 m and 171 m model fundamental from the 83 m fundamental mode at 1.77 Hz and following the experimental data.

The fundamental mode ellipticity curve and TF for each model was produced from the median V_s profile of each corresponding model as shown in Figure 9. The experimental HVSR results of the Manila site along with the ellipticity curve and TF of the 83 m model, 131 m model, and 171 m are demonstrated in Figure 9 (a) through (c), respectively. The experimental HVSR second peak is at 0.85 Hz with a standard deviation of 0.15 Hz. Theoretical ellipticity second peak for 83 m model, 131 m model, and 171 m are respectively 1.23 Hz, 1.12 Hz, and 1.07 Hz, which demonstrates that the difference between the experimental second peak and

23

theoretical ellipticity second peak are decreasing gradually with increasing Memphis sand depth. The resonance frequency from the TF of 83 m model, 131 m model, and 171 m are respectively 0.2333 Hz, 0.2457 Hz, and 0.2436 Hz. The 83 m model, 131 m model, and 171 m model TF resonance frequency have 5.5%, 0.52%, and 1.39% difference with the HVSR fundamental frequency.

Between 131 m model and 171 m model, the former has the lowest minimum misfit, indicating a better fit with the experimental data. The 131 m model was not forced in the first phase of the inversion to resolve the impedance contrast depth, rather it was allowed to search for the best fit. The 131 m model demonstrates the lowest difference between its TF resonance frequency and HVSR fundamental frequency. The approach to generate the 131 m model is practically more suitable as it only needs a tentative idea of the impedance contrast depth but still gives a better result considering the shear wave transfer function.
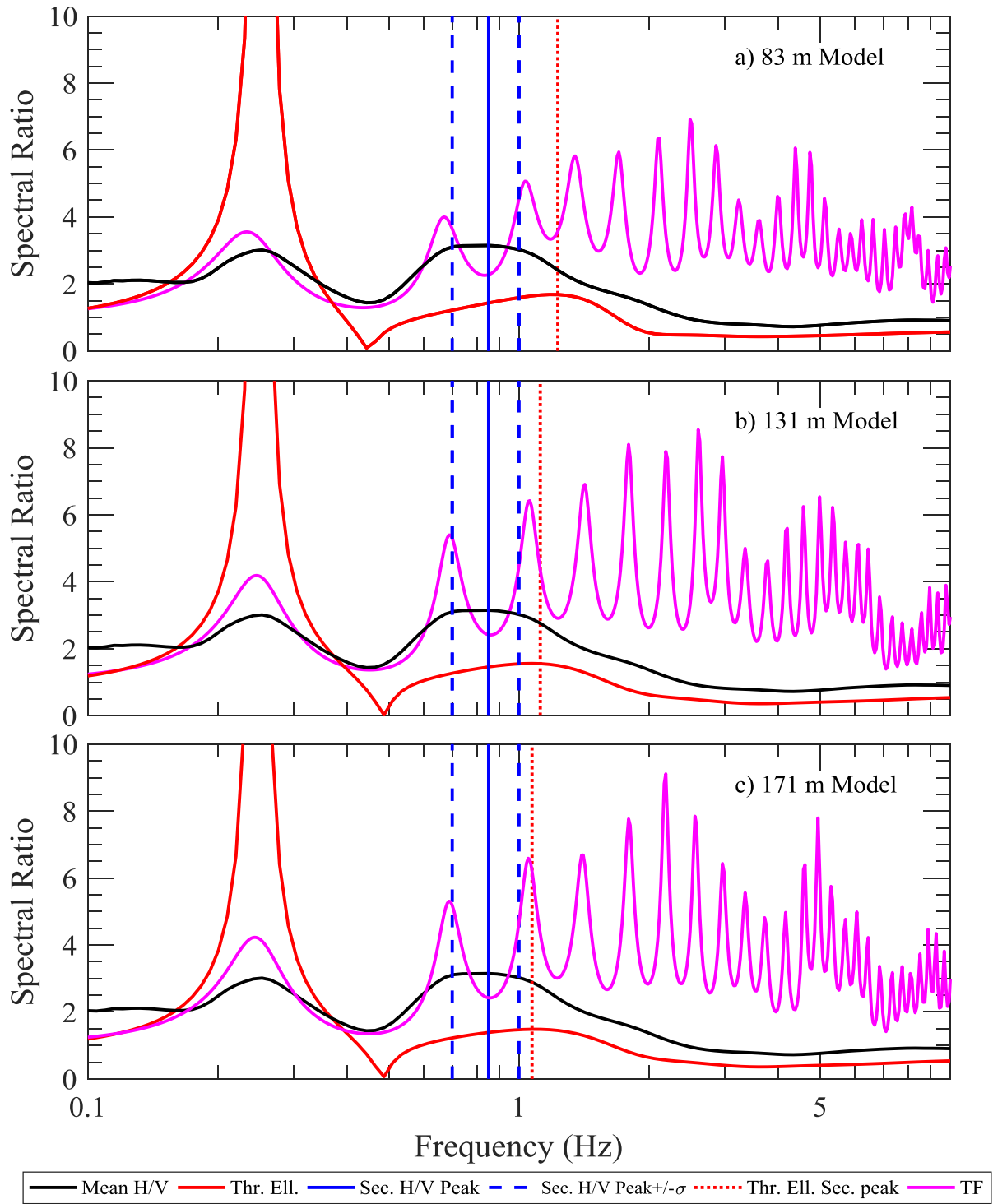
Figure 9: Shear wave transfer function and theoretical ellipticity curve for each model along with the Manila HVSR respectively for the 83 m model (a), 131 m model (b), and 171 m model (c).

6.0 Conclusion:

The horizontal to vertical spectral ratio method was used to estimate the resonance frequency at 15 sites in North East Arkansas. The HVSR results of thirteen sites showed prominent second peak in addition to the fundamental HVSR peak. Shear wave transfer functions were compared for select sites with the HVSR second peaks which indicated poor agreement between the second HVSR peak and the second peak in the shear transfer function for 10 of the 13 sites with second HVSR peaks. In addition, the ratio of f_1/f_0 was shown to be greater than 3 at a majority of the sites reducing the likelihood that an odd harmonic is causing the second HVSR peak. To relate the HVSR results with the Mississippi embayment geology, four seismic stations and an additional five HVSR sites were selected near the northern and western borders of the embayment. The additional HVSR results showed that the HVSR second peak disappeared gradually with the gradual diminishing of Memphis sand layer indicating the second HVSR peak is only present in areas where the Memphis sand exists.

The HVSR second peak was then used along with the fundamental peak and dispersion data to conduct a joint inversion in two phases for a site in Manila, AR. The two V_S models generated in this procedure demonstrates the Memphis sand depth at 131 m and 171 m provides a better fit to the experimental data and borehole information than the estimated depth provided by the CUSVM at 83 meters. This demonstrates the usefulness of including the second HVSR peak in the joint inversion for sites in the Mississippi Embayment.

Applying the new approach of V_S profiling utilizing HVSR second peak for the rest of the NEA sites could be a topic of the future study as the experimental dispersion data for all fifteen North East Arkansas sites are available from Wood *et al.*, 2018.

References:

Ari, H. and Tokimatsu, K., 2005. S-Wave Velocity Profiling by Joint Inversion of Microtremor Dispersion Curve and Horizontal-to-Vertical (H/V) Spectrum, *Bull. Seism. Soc. Am* **95(5)**, 1766–1778, DOI: 10.1785/0120040243.

Bailey, J., P., 2008. Development of shear wave velocity profiles in the deep sediments of the Mississippi Embayment using surface wave and spectral ratio methods, MS Thesis, University of Missouri-Columbia, Columbia.

Bettig, B., Bard, P.Y., Scherbaum, F., Riepl, J., Cotton, F., Cornou, C., and Hatzfield, D., 2001. Analysis of dense array noise measurements using the modified spatial auto correlation method (SPAC): application to the Grenoble area, *Bollettino de Geofisica Teoria e Applicata* **42(3-4)**, 281-304.

Bodin, P., Smith, K., Horton, S., Hwang, H., 2001. Microtremor observations of deep sediment resonance in metropolitan Memphis, Tennessee, *Engineering Geology* **62**, 159-168.

Bonnefoy-Claudet, S., Cornou, C., Bard, P.-Y., Cotton, F., Moczo, P., Kristek, J. & Fah, D., 2006. H/V ratio: a tool for site effects evaluation. Results from 1-D noise simulations, *Geophys. J. Int.* **167**, 827–837.

Bonnefoy-Claudet, S., Kohler, A., Cornou, C., Wathelet, M., Bard, P.-Y., 2008. Effects of love waves on Microtremor H/V ratio, *Bull. Seism. Soc. Am* **98(1)**, 288-300.

Brahana, J.V., Parks, W. S., and Gaydos, M. W., 1987. *Quality of Water from Freshwater Aquifers and Principal Well Fields in the Memphis Area*, Tennessee. USGS Water-Resources Investigations Report 87-4052.

Capon, J., 1969. High Resolution Frequency-Wavenumber Spectrum Analysis, *Proceedings of IEEE* **57(8)**, 1408–1418.

Carpenter, N. S., Wang, Z., Woolery, E. W., Rong, M., 2018. Estimating site response with recordings from deep boreholes and HVSR: examples from the Mississippi embayment of the Central United States, *Bull. Seism. Soc. Am* **108(3A)**, 1199-1209.

Cox, B.R. and Wood, C.M., 2011. Surface Wave Benchmarking Exercise: Methodologies, Results and Uncertainties, in Proceedings, in *Proceedings*, *GeoRisk 2011*, June 26-28, 2011, Atlanta, GA, USA.

Cramer, C. H., 2006. Quantifying the uncertainty in site amplification modeling and its effects on site-specific seismic-hazard estimation in the upper Mississippi embayment and adjacent areas. *Bull. Seism. Soc. Am* **96(6)**, 2008 - 2020.

Cushing, E.M., Boswell, E.H., and Hosman, R.L, 1964. *General geology of the Mississippi Embayment, Water Resources of Mississippi Embayment*, U.S. Geological Survey Professional Paper 448-B.

Dart, R.L., 1995. *Maps of upper Mississippi Embayment Paleozoic and Precambrian Rocks, U.S. Geologic Survey*, Miscellaneous. Field Study Map, MF-2284, 235 - 249.

Deschenes, M. R., Wood, C. M., Himel, A. K., Baker, E., 2019. Development of deep shear wave velocity profiles in Mississippi Embayment. Earthquake Spectra (in review).

DiGiulio, G., Savvaidis, A., Ohrnberger, M., Wathelet, M., Cornou, C., Knapmeyer-Endrun, B., Renalier, F., Theodoulidis, N. and Bard, P.Y., 2012. Exploring the model space and ranking a best class of models in surface-wave dispersion inversion: Application at European strong-motion sites, *Geophysics* **77(3)**, B147–B166.

Dunand, F., et al. 2004. Utilisation du bruit de fond pour l'analyse des dommages des baˆtiments de Boumerdes suite au seˊisme du 21 mai 2003, *Mem. Serv. Geol. Alger*. **12**, 177– 191.

Dunkin, J.W., 1965. Computation of modal solutions in layered, elastic media at high frequencies, *Bull. Seism. Soc.* **55**, 335–358.

Ervin, C. P., and McGinnis, L. D., 1975. Reelfoot Rift: Reactivated precursor to the Mississippi Embayment, *Geol. Soc. Am. Bull*. **86**, 1287 – 1295.

Farrugia, D., Paolucci, E., D'Amico, S., Galea, P., 2016. Inversion of surface wave data for subsurface shear wave velocity profiles characterized by a thick buried low-velocity layer, *Geophysical Journal International*, **206,** 1221-1231.

Field, E., and Jacob, K., 1993. The theoretical response of sedimentary layers to ambient seismic noise, *Geophys. Res. Lett*. **20**, 2925–2928.

Foti, S., Lai, C., Rix, G., and Strobbia, C., 2014. *Surface Wave Methods for Near-Surface Site Characterization*, 1st edition, CRC Press, Boca Raton, FL, 487 pp.

Goetz, R., P., 2009. Study of the horizontal-to-vertical spectral ratio (HVSR) method for characterization of deep soils in the Mississippi Embayment, MS Thesis, University of Missouri-Columbia, Columbia.

Gomberg, J., Waldron, B., Schweig, E., Hwang, H., Webbers, A., Van Arsdale, R., *et al*., 2003. Lithology and shear-wave velocity in Memphis, Tennessee. *Bull. Seism. Soc.* **93 (3)**, 986–997.

Ginzburg, A., Mooney, W. D., Walter, A. D., Lutter, W. J., and Healy, J.H., 1983. Deep structure of the northern Mississippi Embayment, *Bull. Am. Assoc. Petr. Geol.* **67**, 2031-2046.

Guéguen, P., Chatelain, J.-L., Guillier, B., and Yepes, H., and Egred, J., 1998. Site effect and damage distribution in Pujili (Ecuador) after the 28 March 1996 earthquake, *Soil Dyn. Earthq. Eng*. **17**, 329–334.

Guéguen, P., Chatelain, J.-L., Guillier, B., and Yepes, H., 2000. An indication of the soil topmost layer response in Quito (Ecuador) using HVSR spectral ratio, *Soil Dyn. Earthq. Eng*. **19**, 127–133.

Guillier, B., Chatelain, J.-L., Hellel, M., Machane, D., Mezouer, N., Ben Salem, R., 2005. Smooth bumps in H/V curves over a broad area from single-station ambient noise recordings are meaningful and reveal the importance of Q in array processing: The Boumerdes (Algeria) case, *Geophysical Research Letters* **32**, L24306.

Guo, Z., Aydin, A., Kuszmaul, J. S., 2014. Microtremor recordings in Northern Mississippi, *Engineering Geology* **179**, 146-157.

Guo, Z., Aydin, A., 2016. A modified HVSR method to evaluate site effect in Northern Mississippi considering ocean wave climate, *Engineering Geology* **200**, 104-113.

Hashash, Y., Phillips, C., and Groholski, D., 2010. Recent advances in non-linear site response analysis, Paper No. OSP 4, in *Proceedings*, *5th International Conference on Recent Advances in Geotechnical Earthquake Engineering and Soil Dynamics*, 24-29 May, 2010, San Diego, California, USA.

Haskell, N. A., 1953. The dispersion of surface waves on multilayered media, *Bull. Seism. Soc.* **43**, 17–34.

Incorporated Research Institutions for Seismology (IRIS), 2018. Time series data Web page for downloading seismic station data, available at http://ds.iris.edu/ds/nodes/dmc/data/types/waveform-data/ (last accessed July, 2018)

Konno, K., Ohmachi, T., 1998. Ground motion characteristics estimate from spectral ratio between horizontal and vertical components of microtremor, *Bull. Seism. Soc. Am.* **88 (1)**, 228-241.

Lachet, C., D. Hatzfeld, P.-Y. Bard, N. Theodulidis, C. Papaioannou and A. Savvaidis, 1996. Site effects and microzonation in the city of Thessaloniki (Greece): comparison of different approaches, *Bull. Seism. Soc. Am.* **86**, 1692-1703.

Lin, Y. C., Joh, S. H, and Stokoe, K. H., 2014. Analyst J: Analysis of the UTexas 1 Surface Wave Dataset Using the SASW Methodology, Geo-Congress 2014 Technical Papers: Geo-Characterization and Modeling for Sustainability. GSP 234. 2014.

Macau, A., Benjumea, B., Gabàs, A. *et al.*, 2015. The effect of shallow Quaternary deposits on the shape of the H/V spectral ratio, *Surv. Geophys.* **36**, 185-208. https://doi.org/10.1007/s10712-014-9305-z

Mento, D.J., Ervin, C.P., McGinnis, L.D., 1986. Periodic energy release in the New Madrid seismic zone, *Bull. Seism. Soc. Am.* **76**, 1001-1009.

Nakamura, Y., 1989. *A method for dynamic characteristics of subsurface using microtremors on the ground surface*, Quick Report of Railway Technical Research Institute, 30, 25-33.

Nakamura, Y., 2008. On the H/V spectrum, Paper No. 07-0033, *14th World Conference on Earthquake Engineering*, 12–17 October, 2008, Beijing, China.

Ng, K. W., Chang, T. S., Hwang, H., 1989. *Subsurface conditions of Memphis and Shelby County*. Technical report NCEER-89-0021, National Center for Earthquake Research, State University of New York at Buffalo, Buffalo, NY.

Park, C. B., Miller, R. D. & Xia, J., 1999. Multichannel analysis of surface waves, *Geophysics* **64**, 800-880.

Ramírez-Guzmán, L., O., Boyd, S., Hartzell, R., Williams, 2012. Seismic velocity model of the central United States (Version 1): Description and simulation of the 18 April 2008 Mt. Carmel, Illinois, Earthquake, *Bull. Seism. Soc. Am.* **102**, 2622-2645.

Romero, S.M., Rix, G.J., 2005. *Ground Motion Amplification of Soil in the Upper Mississippi Embayment*. GIT-CEE/GEO-01-1, National Science Foundation Mid America Center, Atlanta.

Rosenblad, B., 2008. *Deep shear wave velocity profiles of Mississippi Embayment sediments determined from surface wave measurements*, U.S. Geol. Surv. Final Tech. Rept., USGS NEHRP Award No. 06HQGR0131, 23 pp.

Rosenblad, B., Bailey, J., Csontos, R. and Van Arsdale, R., 2010. Shear Wave Velocities of Mississippi Embayment Soils from Low Frequency Surface Wave Measurements, *Soil Dynamics and Earthquake Engineering* **30**, 691 – 701.

Rosenblad, B., Goetz, R., 2010. Study of the H/V spectral ratio method for determining average shear wave velocities in the Mississippi Embayment, *Engineering Geology* **112**, 13-20.

Ryling, R. W., 1960. *Ground water potential of Mississippi County*, Arkansas, Water Resources Circular, Arkansas Geological Survey, 13-16.

Scherbaum, F., Hinzen, K. G., and Ohrnberger, M., 2003. Determination of shallow shear wave velocity profiles in the Cologne/Germany area using ambient vibrations, *Geophysical Journal International* **152**, 597–612.

Schwalb, H. R., 1971. The northern Mississippi Embayment- A latent Paleozoic oil province, in *Proceedings*, *Symposium on Future Petroleum Potential of NPC Region 9 (Illinois Basin Cincinnati Arch, and Northern Part of Mississippi Embayment)*, 11-12 March, 1971, Champaign, Illinois, USA.

SESAME European project (2004) Guidelines for the Implementation of the H/V Spectral Ratio Technique on Ambient Vibrations: Measurements, Processing and Interpretation. Deliverable D23.12.

Teague, D., Cox, B., Bradley, B. and Wotherspoon, L.M. (2017) Development of Deep Shear Wave Velocity Profiles with Estimates of Uncertainty in the Complex Inter-Bedded Geology of Christchurch, in review.

Teague, D. P., Cox, B. R., Rathje, E. M., 2018. Measured vs. predicted site response at the Garner valley downhole array considering shear wave velocity uncertainty from borehole and surface wave methods, *Soil Dynamics and Earthquake Engineering* **113**, 339-355

Thomson, W. T., 1950. Transmission of elastic waves through a stratified solid medium, *Journal of Applied Physics* **21**, 89–93.

Van Arsdale, R.B., TenBrink, R.K., 2000. Late Cretaceous and Cenozoic Geology of the New Madrid Seismic Zone, *Bull. Seism. Soc. Am.* **90**, 345–356.

Wathelet, M., 2008. An improved neighborhood algorithm: parameter conditions and dynamic scaling, *Geophysical Research Letters* **35**, L09301.

Williams, R. A., Wood, S., Stephenson, W. J., *et al*., 2003. Surface seismic refraction/reflection measurement determinations of potential site resonances and the areal uniformity of NEHRP site class D in Memphis, Tennessee. *Earthquake Spectra* **19 (1)**, 159-89.

Wood, C. M., Baker, E., Deschenes, M., Himel, A. K., 2018. Deep shear wave velocity profiling in Northeastern Arkansas, TRC 1603, Arkansas Department of Transportation.

Wotherspoon, L.M., Munro, J., Bradley, B.A., Wood, C.M., Thompson, E., Deschenes, M., Cox, B. (2018). Site period characteristics across the Canterbury region of New Zealand, GEESD conference, Austin TX, June 2018.

Woolery, E. W., Wang, Z., Carpenter, N. S., Street, R., Brengman, C., 2016. The Central United States Seismic Observatory: Site Characterization, Instrumentation, and Recordings. *Seismological Research Letters* 87 (1), 215–228. https://doi.org/10.1785/0220150169

Zaslavsky, Y., et al., 2007. Use of ambient vibration measurements for reconstruction of subsurface structure along three profiles in the Zevulun Plain, Report No 571/240/07, The Geophysical institute of Israel.

Zywicki, D.J., 1999. Advanced signal processing methods applied to engineering analysis of seismic surface waves, Ph.D. Dissertation, School of Civil and Environmental Engineering, Georgia Institute of Technology, Atlanta, GA.